

Spatio-temporal evolution of global surface temperature distributions

Federico Amato^{1,*}, Fabian Guignard¹, Vincent Humphrey², and Mikhail Kanevski¹

¹University of Lausanne, Faculty of Geosciences and Environment, IDYST, UNIL - Geopolis, 1015 Lausanne, Switzerland

²California Institute of Technology, Pasadena, United States

*federico.amato@unil.ch

ABSTRACT

Climate is known for being characterised by strong non-linearity and chaotic behaviour. Nevertheless, few studies in climate science adopt statistical methods specifically designed for non-stationary or non-linear systems. Here we show how the use of statistical methods from Information Theory can describe the non-stationary behaviour of climate fields, unveiling spatial and temporal patterns that may otherwise be difficult to recognize. We study the maximum temperature at two meters above ground using the NCEP CDAS1 daily reanalysis data, with a spatial resolution of 2.5° by 2.5° and covering the time period from 1 January 1948 to 30 November 2018. The spatial and temporal evolution of the temperature time series are retrieved using the Fisher Information Measure, which quantifies the information in a signal, and the Shannon Entropy Power, which is a measure of its uncertainty — or unpredictability. The results describe the temporal behaviour of the analysed variable. Our findings suggest that tropical and temperate zones are now characterized by higher levels of entropy. Finally, Fisher-Shannon Complexity is introduced and applied to study the evolution of the daily maximum surface temperature distributions.

Motivation

In the context of anthropogenic greenhouse gas emissions, global climate has been the focus of extensive research over the last decades. Countries which have adhered to the 2016 Paris Agreement aim to limit the increase in global average temperature below 1.5°C and mitigate the risks and impacts of climate change¹. Moreover, climate change is also a primary concern in the context of the Sustainable Development Goals (SDGs)². In the United Nations agenda, climate influence on sustainable development is closely related not only to environmental issues but also to the social and economic dimension of the SDGs. Similarly, the Intergovernmental Panel on Climate Change (IPCC) has investigated the interaction between sustainable development, poverty eradication and ethics and equity³. Many of these interactions are related to the fact that warming has significant spatial and temporal patterns that could affect some regions more than others. As an example many locations, especially in the Northern Hemisphere at the mid-latitudes, are experiencing regional warming that is more than double the global average⁴.

Because climate is characterised by strong nonlinearity and chaotic behaviour, many studies in climate science cannot rely on statistical methods valid only for stationary or linear systems^{5,6}. It has already been shown that warming trends are characterised by strong non-linearities, with an acceleration in the increase of temperatures since 1980⁷.

In the present research we attempt to further investigate the complex nature of surface temperature, showing how statistical methods from Information Theory can be used to describe the non-stationary behaviour of such phenomena. We study the maximum temperature at two meters above ground using the NCEP CDAS1 daily reanalysis data, with a spatial resolution of 2.5° by 2.5° and covering the time period from 1 January 1948 to 30 November 2018⁸. For each spatial location we track through a sliding window the evolution of the corresponding temperature time series using the Fisher Information Measure (FIM)⁹, which is a powerful tool to identify the behaviour of dynamical systems, and the Shannon Entropy Power (SEP)¹⁰, which can be used to quantify the uncertainty — or the disorder — of a signal. We show how these measures can be used to retrieve the spatial and temporal changes of the investigated time series distributions, highlighting the complex behaviour of the temperature spatio-temporal field.

Methods

This section provides details concerning the estimation of FIM and SEP. Briefly, FIM is used to measure the information in a given signal x , while SEP quantifies its degree of disorder and predictability. To unveil the spatial structures of the

spatio-temporal values of FIM and SEP computed, an Empirical Orthogonal Function (EOF) decomposition will also be performed on the data of the two estimations. EOF analysis is the spatio-temporal version of principal component analysis. Through this approach, data are decomposed into orthogonal basis functions defined by spatial eigenvectors — the Empirical Orthogonal Functions (EOFs) — and temporal coefficients described by the principal components (PC) time series.

Fisher Information Measure and Shannon Entropy Power

SEP and FIM are summary quantities to partially describe a Probability Density Function (PDF). Let X be an univariate continuous random variable following a PDF $f(x)$. The SEP of X is defined as N_X through the relationship¹¹

$$N_X = \frac{1}{2\pi e} e^{2H_X}, \quad H_X = \mathbb{E}[-\log f(x)]. \quad (1)$$

The SEP is a strictly increasing transformation of H_X , which is the differential entropy of X ¹². The FIM of X , noted I_X , is defined as¹¹.

$$I_X = \mathbb{E} \left[\left(\frac{\partial}{\partial x} \log f(X) \right)^2 \right]. \quad (2)$$

SEP and FIM can be jointly visualized into the Fisher-Shannon Information Plane (FSIP) to study the PDF of X ^{13,14}. It can be shown that $N_X \cdot I_X \geq 1$, with the equality satisfied if and only if X is a Gaussian random variable¹¹. Hence, the only reachable points in the FSIP belong to the set

$$\mathcal{D} = \left\{ (N_X, I_X) \in \mathbb{R}^2 \mid \begin{array}{l} N_X > 0, I_X > 0, \\ N_X \cdot I_X \geq 1 \end{array} \right\}.$$

The quantity $C_X = N_X \cdot I_X$, which is called Fisher-Shannon Complexity (FSC), is sometimes used as a statistical complexity measure^{15,16}.

It has been shown that the FSC can be interpreted as a measure of non-Gaussianness of X ¹⁴. Thus, the boundary of \mathcal{D} is reached if and only if X has a unitary FSC, in which case it is a Gaussian random variable.

In order to estimate SEP and FIM from data, $f(x)$ and its derivative $f'(x)$ were replaced by their kernel density estimators (KDE) in the integral forms of (1) and (2),¹⁷⁻²¹. To this aim, given n independent realizations $\{x_1, \dots, x_n\}$ of X , the PDF $f(x)$ is approximated as²²

$$\hat{f}_h(x) = \frac{1}{nh} \sum_{i=1}^n K\left(\frac{x-x_i}{h}\right), \quad (3)$$

where h is a bandwidth parameter and $K(\cdot)$ is a kernel assumed to be a unimodal probability density function symmetric around zero and having integral over \mathbb{R} equal to 1. By using a Gaussian kernel with zero mean and unit variance, the estimator (3) assumes the form

$$\hat{f}_h(x) = \frac{1}{nh\sqrt{2\pi}} \sum_{i=1}^n e^{-\frac{1}{2}\left(\frac{x-x_i}{h}\right)^2}. \quad (4)$$

By deriving $\hat{f}_h(x)$ one can estimate the PDF derivative $f'(x)$ as

$$\hat{f}'_h(x) = \frac{1}{nh^3\sqrt{2\pi}} \sum_{i=1}^n (x-x_i) e^{-\frac{1}{2}\left(\frac{x-x_i}{h}\right)^2}. \quad (5)$$

By plugging estimates (4) and (5) into the equations (1) and (2), the latter assumes the form

$$\hat{N}_X = \frac{1}{2\pi e} e^{-2 \int \hat{f}_h(x) \log \hat{f}_h(x) dx},$$

and

$$\hat{I}_X = \int \frac{(\hat{f}'_h(x))^2}{\hat{f}_h(x)} dx.$$

The FSC is estimated by multiplying \hat{N}_X by \hat{I}_X . The estimates are sensitive to the choice of a proper bandwidth. Here, this parameter is selected using the Sheather-Jones direct plug-in method²³, which approximates the optimal bandwidth with respect to the Asymptotic Mean Integrated Squared Error of \hat{f}_h . Operationally, the non-parametric estimation of the SEP, FIM and FSC are obtained with the FiShPy package¹⁴.

Empirical Orthogonal Functions

EOF analysis is an extremely popular approach to study the variability in a geophysical field of interest²⁴. EOF analysis can be seen as an application of Principal Component Analysis in the case where data is a multivariate spatially indexed vector with multiple samples over time^{25,26}.

Let $\mathbf{X}_{t_j} = (X(\mathbf{s}_1; t_j), \dots, X(\mathbf{s}_m; t_j))' \in \mathbb{R}^m$ be observations for the spatial locations $\{\mathbf{s}_i : i = 1, \dots, m\}$ and times $\{t_j : j = 1, \dots, T\}$. The empirical spatial mean for all location is given by

$$\hat{\boldsymbol{\mu}} = \frac{1}{T} \sum_{j=1}^T \mathbf{X}_{t_j}.$$

The empirical spatial covariance matrix²⁷ can then be computed as

$$\hat{\mathbf{C}} = \frac{1}{T} \sum_{j=1}^T (\mathbf{X}_{t_j} - \hat{\boldsymbol{\mu}})(\mathbf{X}_{t_j} - \hat{\boldsymbol{\mu}})'$$

As this real matrix is symmetric and non-negative definite, it can be spectrally decomposed as

$$\hat{\mathbf{C}} = \Phi \Lambda \Phi'$$

where $\Lambda = \text{diag}(\lambda_1, \dots, \lambda_m)$ is the diagonal matrix of the non-negative eigenvalues decreasing down the diagonal, and $\Phi = (\phi_1, \dots, \phi_m)$ is the matrix of the corresponding spatially indexed eigenvectors $\phi_k = (\phi_k(\mathbf{s}_1), \dots, \phi_k(\mathbf{s}_m))'$, for $k = 1, \dots, m$, also called EOFs. The EOFs form a discrete orthonormal basis²⁸. The k -th PC time series — which is the time series of coefficient of the corresponding EOF, or equivalently the contribution of the k -th spatial basis at time t_j — is then given by $a_k(t_j) = \phi_k' \mathbf{X}_{t_j}$ ²⁹.

Results

Temporal changes of temperature distributions

To study the NCEP CDAS1 daily data, we first consider separately the temperature time series of the single spatial locations. For each of them, we computed time-dependent measures of SEP and FIM using a sliding temporal window of width equal to five years and a sliding factor equal to one month.

To make spatial and temporal variabilities comparable, the obtained measures for each location have been standardized with a z-score transformation. The spatial distribution of FIM and SEP shown in Figure 1 highlights two different behaviour. In the

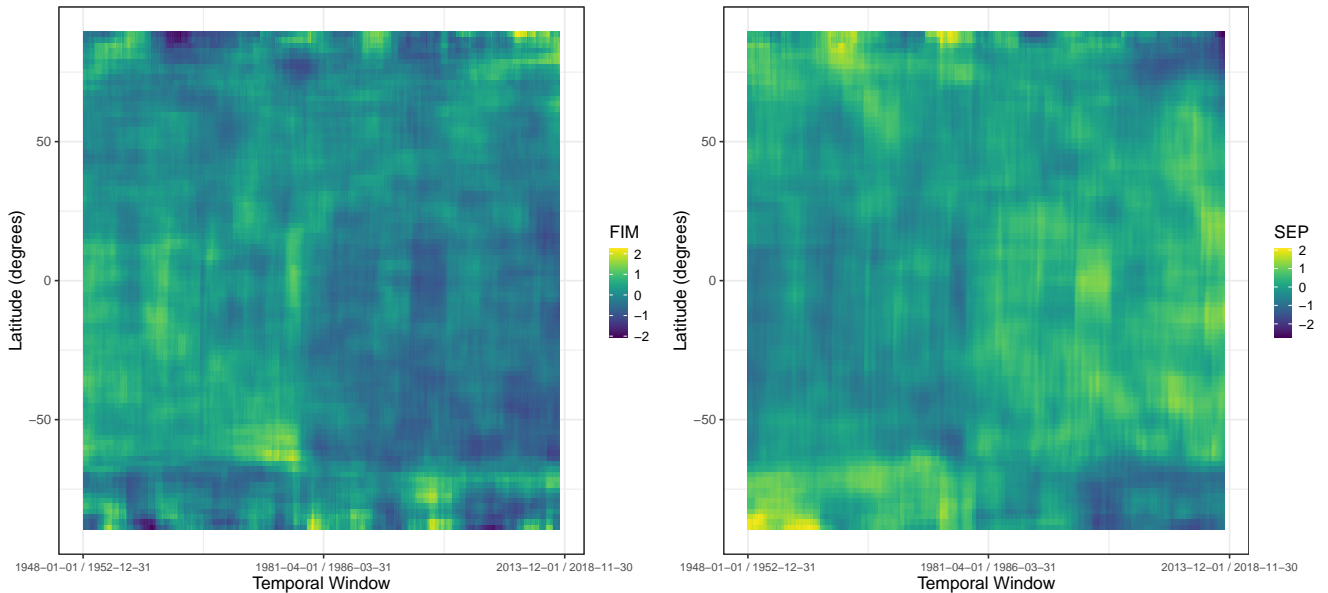


Figure 1. Hovmöller plots for the latitude for both FIM and SEP. The figures represent the mean values of the two measures over land and oceans. Data have been standardized using a z-score transformation.

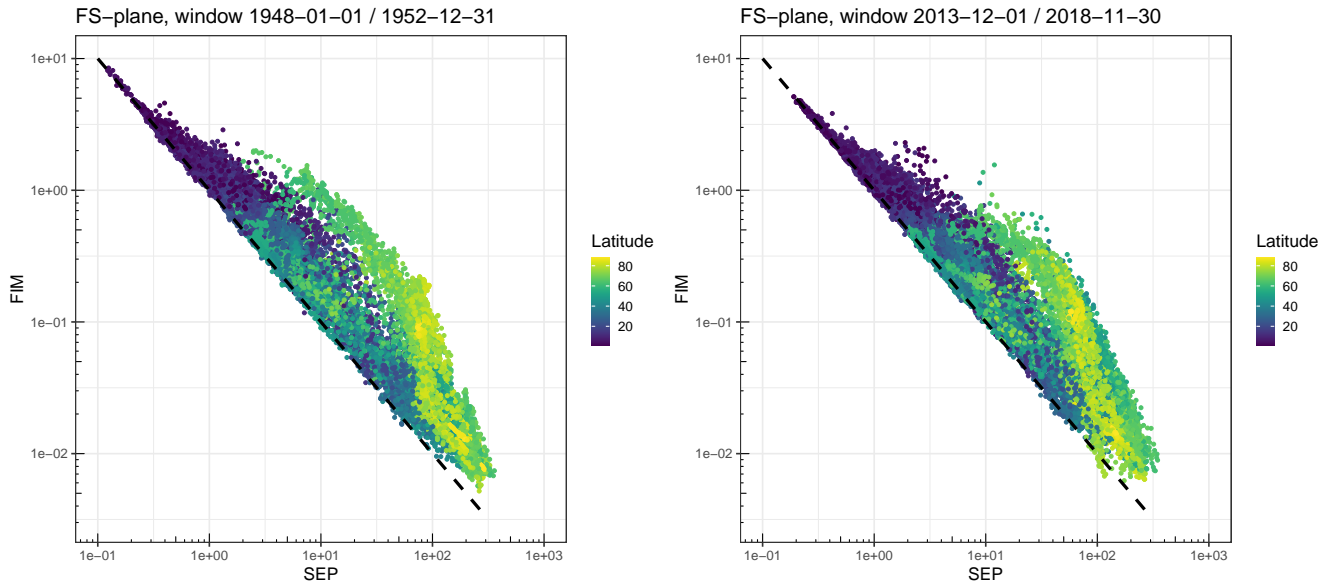


Figure 2. Fisher-Shannon Information Plane. The FSIP constructed with the estimated values of FIM and SEP for the first (left) and last (right) sliding windows. Each point corresponds to a spatial location, while the dashed line represents the theoretical Gaussian limit. Color indicates the absolute value of the latitude of the points.

period from 1948 to 1979 the latitudes higher than 60° and lower than -60° are characterized by high levels of SEP and low levels of FIM. The situation has completely reversed starting from 1979, and in a faster way for the latitudes higher than 60° , so that tropical and temperate zones are now characterized by higher levels of entropy. The northern mid-latitude seems to have slightly stronger growth of SEP.

The FSIP is used for a simultaneous analysis of FIM and SEP to track the non-stationary behaviour of the temperature time series¹³. Figure 2 shows the FSIP of the non z-scored data for the first sliding window (from 1948/01/01 to 1952/12/31) and for the last one (from 2013/12/01 to 2018/11/30). The Figure highlights how the characterization of points in the FSIP is strongly linked to their latitude. The latitudes higher than 60° and lower than -60° are easily recognizable for having a behaviour more distant from the one expected in the Gaussian case. Moreover, it is possible to observe a significant movement of these points from the first to the last window. The displacements of the points in the plane can be interpreted as a change of the distribution of temperature.

FSC is analyzed in Figure 3. The Hovmöller plot highlights how the equatorial areas exhibit a FSC fluctuating around values not far from 1, implying temperature distributions almost Gaussian. Latitudes higher than $60^\circ N$ and lower than $-60^\circ S$ show a reduction of the FSC over time. Figure 3 also investigates the FSC of the point having Longitude = 232.0 and Latitude = 56.2, located in the western Canada. This is one of the point experiencing the greater overall change in the measured complexity over time among all the investigated spatial locations. The distribution changes of temperature at this location is clearly observed in the FSIP. The trajectory defined in the plane highlights different stages in its behaviour, which is also recognizable in the timeseries of the FSC. The latter show decreasing complexity values since September 1989. FSC can be used as a clear indicator of a changing pattern in the distribution of data. As an example, three distributions are shown, computed on the temporal windows from 1951-12-01 to 1956-11-0, from 1989-09-01 to 1994-08-31 and from 2009-02-01 to 2014-01-31, respectively. All the distributions exhibit bimodality, where the modes are determined by the seasonals variabilities. The first distribution, associated with a FSC of 3.32, is actually not far from being a mixture of two Gaussian distributions. Indeed, it can be empirically observed that for a mixture of two Gaussian distributions having the same variance, the FSC goes to 4 when the modes move away from each other. Differently, the second distribution plot, corresponding to an FSC of 29.37, is dominated by the mode at 273K. This is still true in the last plot, corresponding to FSC of 6.67, although since September 1989 a reduction of the complexity has been registered, indicating a behaviour closer to Gaussian.

Regional behaviour of temperature distributions

To further improve the understanding of the spatial patterns of the variability in the spatio-temporal values of the estimated SEP and FIM, EOF decompositions were performed. Figure 4 shows the first two EOFs and the corresponding PC time series for both SEP and FIM estimates.

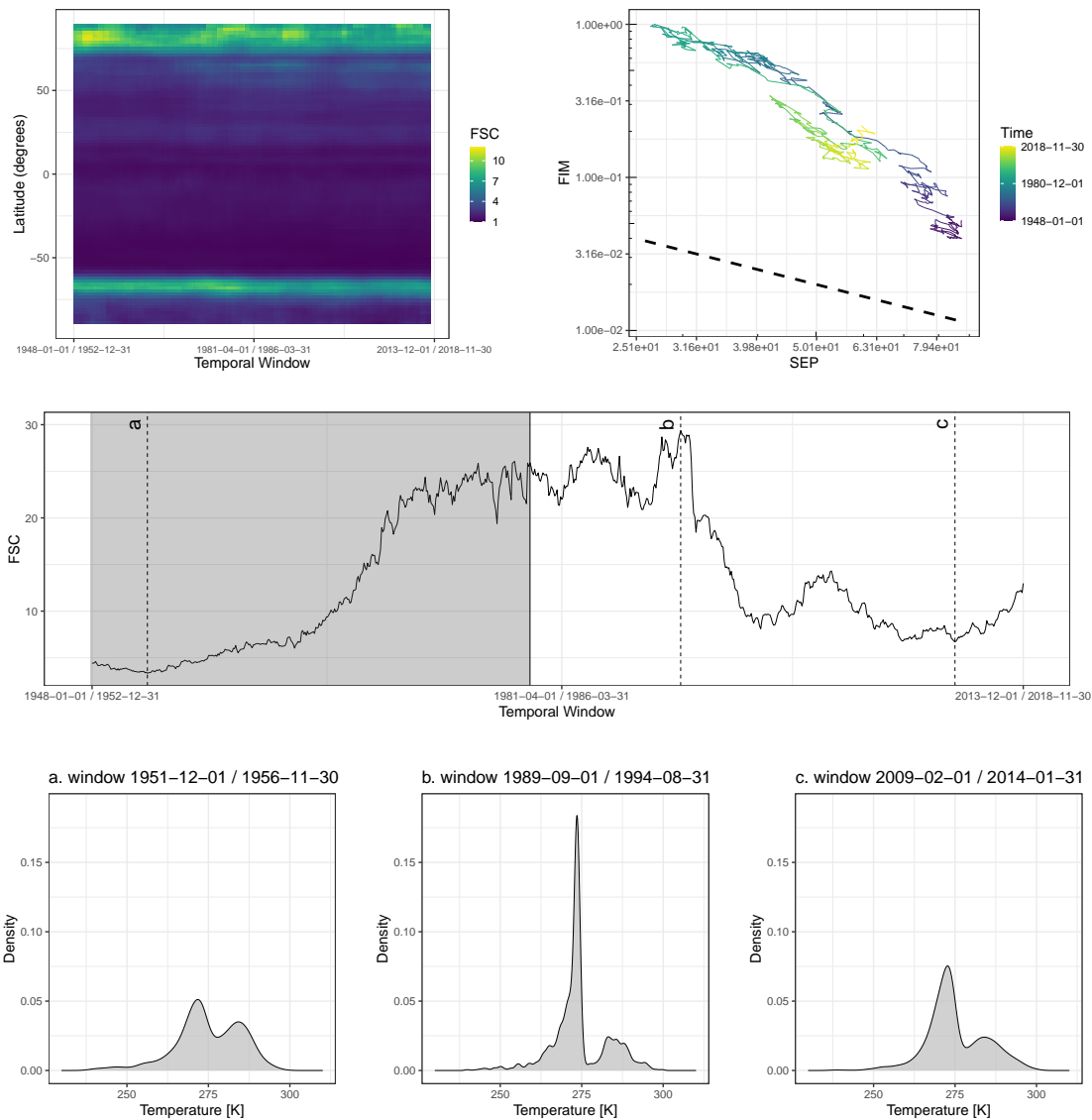


Figure 3. Fisher-Shannon Complexity. Top left: Hovmöller latitudinal plot for FSC. Top right: Trajectory in the FSIP of the point represented by a red triangle in Figure 4 and having Longitude = 232.0 and Latitude = 56.2. The dashed line represents the theoretical Gaussian limit. Middle: FSC of the same point over time. The grey region covers the temporal period from 1948-01-01 to 1979-01-01. Bottom row: Distributions of the temperature measurements in the temporal windows resulting into the FSC points highlighted with a vertical dashed line in the previous plot.

The first EOFs reproduce the pattern of reduction of SEP and growth of FIM in the extreme northern and southern latitudes. The first EOFs also show a drastic difference between oceans and lands surfaces, with the former generally characterized by significant increases of SEP in the period after 1979. This may be related to the fact that the land surface experiences a stronger warming than the ocean surface, in relation to the higher evaporation and heat storage capacity of the oceans³⁰. It might also be related to changes in the atmospheric circulation (e.g. the North Atlantic oscillation and the related arctic oscillation). This pattern might also reflect some spatial properties of the observing system. Because weather stations and atmospheric soundings are typically land-based, the atmospheric reanalysis assimilates much more observations over land than over the ocean, particularly until the first satellite observations became available in 1979. The PC time series corresponding to the first EOFs show how the data are increasingly projecting on these spatial patterns starting from 1979.

The second EOFs for SEP and FIM highlight interesting spatial patterns, once again related to significant changes starting from the late eighties as it shown by the corresponding PC time series. The most evident spatial trends concern the continental

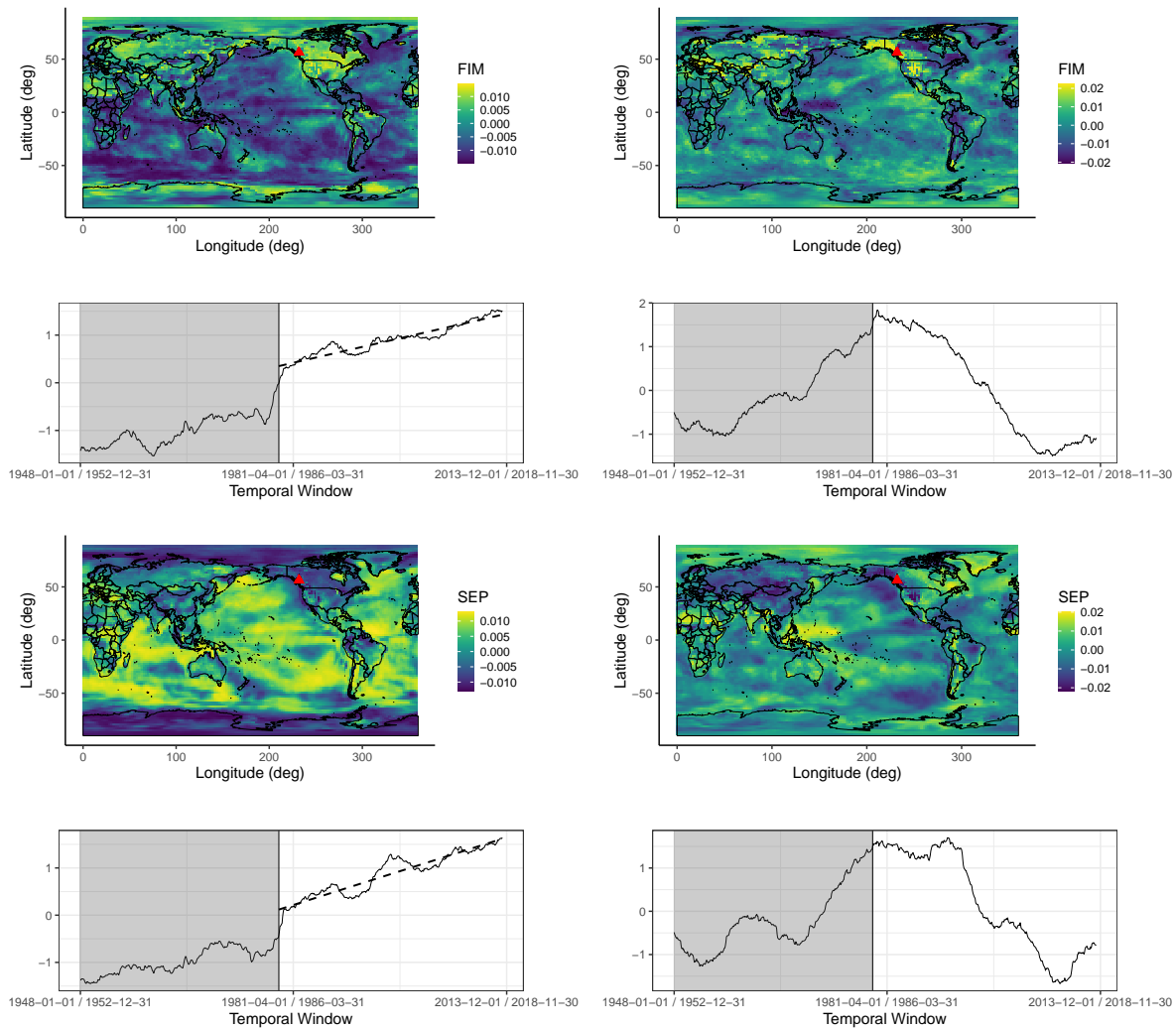


Figure 4. Empirical Orthogonal Function decomposition. First two EOFs and corresponding PC time series for the FIM (top) and the SEP (bottom). The red triangle in the maps corresponds to the point explored in Figure 3. The grey regions in the PC time series plots cover the temporal period from 1948-01-01 to 1979-01-01. For the PC time series corresponding to the first components, a regression line is fitted to the data from January 1979 and reported with a dashed line.

interiors of Asia, the western North America and central Brazil. These regions are described in the second EOFs by growing values of FIM up to the late eighties, with a drastic change from that period onward.

Conclusions

This paper discussed how statistical methods derived from Information Theory could be used to investigate the properties of a climate field, specifically the surface air temperature. We found that the three measures applied, FIM, SEP and FSC, could provide meaningful insight about the global and local properties of the mentioned time series. Specifically, we were able to recover spatio-temporal structures in the data, depicting behaviours that, otherwise, would have been difficult to highlight.

Indeed, the results presented in the previous section underpin the capability of the applied measures to detect the degree to which observational products, such as the reanalyses ones, are affected by step changes in the underlying observing system. The detection of such changes is relevant, as a lack of their documentation may lead scientist to misleading conclusions regarding, for instance, climate trends. An example is the detection of two phases in the reanalysis dataset studied in this paper. The two are clearly separated by a behavioural change in 1979 recognized by both FIM and SEP. Indeed, starting from 1980 with the introduction of the Operational Vertical Sounder (TVOS), satellite data became part of the reanalysis model. The PC time series

in Figure 4 are particularly effective to visualize this changing point. Nonetheless, even just considering data from 1979 it is possible to clearly identify spatial and temporal patterns in the two measures computed - as shown in Figure 4 by the regression lines on the PC time series of the first components of SEP ($R^2 = 0.889$) and FIM ($R^2 = 0.902$).

Warming is not a smooth monotonous process, and the chaotic nature of climate systems reduces the possibility of performing reliable forecasts of future temperature scenarios³¹. Previous studies shown that entropy can be used to spatially identify unpredictability patterns in surface temperature data³². The joint use of SEP and FIM highlighted how the spatial and temporal evolution of this predictability level may not be constant over the entire globe and along time, stressing how the increase of observational data could not always lead to a decrease of such unpredictability³³. However, the effect of the distribution changes along time on the medium to long term forecasts will have to be further investigated.

Future work will also have to focus on the study of the trend recognized in SEP and FIM since 1979. It is not possible to infer the causal factors inducing this trend using only the NCEP CDAS1 data, as it is not possible to distinguish the effects induced by the growing number of available observations used by the model and those caused by a changing climate. Hence, future analysis will be based on factorial climate simulations from the Coupled Model Intercomparison Project, to compare the information/entropy behaviour of pre-industrial control simulations versus historical simulations including the effects of land use change and greenhouse gas emissions. This could recognize specific patterns due to e.g. GHG emissions.

Acknowledgments

The research presented in this paper was partly supported by the National Research Program 75 "Big Data" (PNR75, project No. 167285 "HyEnergy") of the Swiss National Science Foundation (SNSF). V.H. is supported by the SNSF grant no. P400P2_180784.

References

1. Hulme, M. 1.5°C and climate research after the paris agreement. *Nat. Clim. Chang.* **6**, 222 (2016).
2. GA, U. Transforming our world: the 2030 agenda for sustainable development. *Div. for Sustain. Dev. Goals: New York, NY, USA* (2015).
3. IPCC. *Global Warming of 1.5°C : An IPCC Special Report on the Impacts of Global Warming of 1.5°C Above Pre-industrial Levels and Related Global Greenhouse Gas Emission Pathways, in the Context of Strengthening the Global Response to the Threat of Climate Change, Sustainable Development, and Efforts to Eradicate Poverty* (Intergovernmental Panel on Climate Change, 2018).
4. Collins, M. *et al.* Long-term climate change: projections, commitments and irreversibility. In *Climate Change 2013-The Physical Science Basis: Contribution of Working Group I to the Fifth Assessment Report of the Intergovernmental Panel on Climate Change*, 1029–1136 (Cambridge University Press, 2013).
5. Franzke, C. L. Warming trends: nonlinear climate change. *Nat. Clim. Chang.* **4**, 423 (2014).
6. Ribes, A., Thao, S. & Cattiaux, J. Describing the relationship between a weather event and climate change: a new statistical approach. *J. Clim.* (2020).
7. Ji, F., Wu, Z., Huang, J. & Chassignet, E. P. Evolution of land surface air temperature trend. *Nat. Clim. Chang.* **4**, 462 (2014).
8. Kalnay, E. *et al.* The ncep/ncar 40-year reanalysis project. *Bull. Am. meteorological Soc.* **77**, 437–472 (1996).
9. Fisher, R. A. Theory of statistical estimation. *Math. Proc. Camb. Philos. Soc.* **22**, 700–725, DOI: [10.1017/S0305004100009580](https://doi.org/10.1017/S0305004100009580) (1925).
10. Shannon, C. E. A mathematical theory of communication. *Bell Syst. Tech. J.* **27**, 379–423, DOI: [10.1002/j.1538-7305.1948.tb01338.x](https://doi.org/10.1002/j.1538-7305.1948.tb01338.x) (1948).
11. Dembo, A., Cover, T. M. & Thomas, J. A. Information theoretic inequalities. *IEEE Transactions on Inf. Theory* **37**, 1501–1518, DOI: [10.1109/18.104312](https://doi.org/10.1109/18.104312) (1991).
12. Cover, T. M. & Thomas, J. A. *Elements of Information Theory (Wiley Series in Telecommunications and Signal Processing)* (Wiley-Interscience, New York, NY, USA, 2006).
13. Vignat, C. & Bercher, J.-F. Analysis of signals in the fisher–shannon information plane. *Phys. Lett. A* **312**, 27 – 33, DOI: [https://doi.org/10.1016/S0375-9601\(03\)00570-X](https://doi.org/10.1016/S0375-9601(03)00570-X) (2003).
14. Guignard, F., Laib, M., Amato, F. & Kanevski, M. Advanced analysis of temporal data using Fisher-Shannon information: theoretical development and application in geosciences. *Front. Earth Sci.* (2020).

15. Angulo, J., Antolín, J. & Sen, K. Fisher–Shannon plane and statistical complexity of atoms. *Phys. Lett. A* **372**, 670 – 674, DOI: <https://doi.org/10.1016/j.physleta.2007.07.077> (2008).
16. Esquivel, R. O. *et al.* Analysis of complexity measures and information planes of selected molecules in position and momentum spaces. *Phys. Chem. Chem. Phys.* **12**, 7108–7116, DOI: [10.1039/B927055H](https://doi.org/10.1039/B927055H) (2010).
17. Bhattacharya, P. K. Estimation of a probability density function and its derivatives. *The Indian J. Stat. Ser. A (1961-2002)* **29**, 373–382 (1967).
18. Dmitriev, Y. & Tarasenko, F. On the estimation of functionals of the probability density and its derivatives. *Theory Probab. & Its Appl.* **18**, 628–633, DOI: [10.1137/1118083](https://doi.org/10.1137/1118083) (1973).
19. Prakasa Rao, B. *Nonparametric Functional Estimation*. Probability and Mathematical Statistics: A Series of Monographs and Textbooks (Academic Press, 1983).
20. Györfi, L. & van der Meulen, E. C. Density-free convergence properties of various estimators of entropy. *Comput. Stat. Data Analysis* **5**, 425 – 436, DOI: [https://doi.org/10.1016/0167-9473\(87\)90065-X](https://doi.org/10.1016/0167-9473(87)90065-X) (1987).
21. Joe, H. Estimation of entropy and other functionals of a multivariate density. *Annals Inst. Stat. Math.* **41**, 683–697, DOI: [10.1007/BF00057735](https://doi.org/10.1007/BF00057735) (1989).
22. Wand, M. & Jones, M. *Kernel Smoothing*. Chapman & Hall/CRC Monographs on Statistics & Applied Probability (Taylor & Francis, 1994).
23. Sheather, S. J. & Jones, M. C. A reliable data-based bandwidth selection method for kernel density estimation. *J. Royal Stat. Soc. Ser. B (Methodological)* **53**, 683–690 (1991).
24. Hannachi, A., Jolliffe, I. & Stephenson, D. Empirical orthogonal functions and related techniques in atmospheric science: A review. *Int. J. Climatol. A J. Royal Meteorol. Soc.* **27**, 1119–1152 (2007).
25. Lorenz, E. N. Empirical orthogonal functions and statistical weather prediction. *Mass. Inst. Technol. Dep. Meteorol. Camb.* (1956).
26. Jolliffe, I. T. & Cadima, J. Principal component analysis: a review and recent developments. *Philos. Transactions Royal Soc. A: Math. Phys. Eng. Sci.* **374**, 20150202 (2016).
27. Wikle, C. K., Zammit-Mangion, A. & Cressie, N. *Spatio-temporal Statistics with R* (CRC Press, 2019).
28. Cressie, N. & Wikle, C. K. *Statistics for spatio-temporal data* (John Wiley & Sons, 2015).
29. Monahan, A. H., Fyfe, J. C., Ambaum, M. H., Stephenson, D. B. & North, G. R. Empirical orthogonal functions: The medium is the message. *J. Clim.* **22**, 6501–6514 (2009).
30. Guemas, V., Doblas-Reyes, F. J., Andreu-Burillo, I. & Asif, M. Retrospective prediction of the global warming slowdown in the past decade. *Nat. Clim. Chang.* **3**, 649 (2013).
31. Sévellec, F. & Drijfhout, S. S. A novel probabilistic forecast system predicting anomalously warm 2018-2022 reinforcing the long-term global warming trend. *Nat. communications* **9**, 3024 (2018).
32. Arizmendi, F., Barreiro, M. & Masoller, C. Identifying large-scale patterns of unpredictability and response to insolation in atmospheric data. *Sci. reports* **7**, 45676 (2017).
33. Zidek, J. V. & van Eeden, C. Uncertainty, entropy, variance and the effect of partial information. *Lect. Notes-Monograph Ser.* 155–167 (2003).